Design and experiment of low-damage and high-cleanliness segmented combined peeling roller for maize peeling device

Zhenye Li[1,2], Jun Fu[1,2], Zhao Xue[1,2*], Qiankun Fu[1,2], Xiwen Luo[3]

(1. *College of Biological and Agricultural Engineering, Jilin University, Changchun 130022, China*;
2. *Key Laboratory of Efficient Sowing and Harvesting Equipment, Ministry of Agriculture and Rural Affairs, Jilin University, Changchun 130022, China*;
3. *College of Engineering, South China Agricultural University, Guangzhou 510642, China*)

Abstract: Aiming at the key technical bottleneck that the high bract stripping rate and low grain damage rate are mutually restricted during the peeling process of maize ear harvesters, a segmented combined peeling roller was designed to achieve the operational goal of "low damage and high cleanliness". By establishing the contact mechanical model between the convex ribs and the maize ear and analyzing the dynamic process of maize ear peeling, the arc convex rib-groove structure and the three-section combined configuration were determined, which realized graded adaptation and low-damage, high-cleanliness operation in the peeling process. Friction characteristic tests, simulation tests, orthogonal optimization tests, and field verification tests were carried out. The results showed that the rolling friction coefficient and contact stress between the segmented combined peeling roller and the maize ear decreased sequentially from the front section to the rear section. Using the Box-Behnken response surface method to optimize the operating parameters, the optimal parameter combination was obtained: the peeling roller speed was 353 r/min, the pressing wheel speed was 82 r/min, and the distance between the peeling roller and pressing wheel was 31 mm. Compared with the conventional fish-scale spiral peeling roller, the bract stripping rate of the designed segmented combined peeling roller was increased by 10.89%, while the grain shedding rate and grain breaking rate were reduced by 68.93% and 63.51%, respectively. This study provides theoretical support and engineering reference for the optimal design of the low-damage and high-cleanliness maize peeling devices.

Keywords: maize, mechanical peeling, peeling roller, low damage and high cleanliness, segmented combined
DOI: 10.25165/j.ijabe.20261904.9836

Citation: Li Z Y, Fu J, Xue Z, Fu Q K, Luo X W. Design and experiment of low-damage and high-cleanliness segmented combined peeling roller for maize peeling device. Int J Agric & Biol Eng, 2026; 19(4): 88–97.

1 Introduction

Mechanical peeling of maize ears is a critical process in mechanized maize harvesting, and its operational performance directly determines the harvesting quality and post-harvest storage quality[1,2]. In China, the kernel moisture content of maize during the harvesting period is generally high, reaching even 30%-40% in some regions[3]. Under high-humidity conditions, the bracts are tightly wrapped with strong fiber toughness, and the maize kernels are soft in texture, which easily causes incomplete bract stripping and kernel extrusion damage[4,5]. Currently, the difficulty in synergistically balancing high bract stripping rate and low grain damage rate during peeling operations has become a key bottleneck restricting the reduction of losses and efficiency improvement in mechanized maize harvesting[6,7]. Therefore, conducting research on low-damage and high-cleanliness mechanical peeling technology for high-humidity maize is of great engineering application value.

Received date: 2025-04-08 **Accepted date:** 2026-05-15

Biographies: Zhenye Li, PhD, Assistant Researcher, research interest: modern agricultural equipment technology, Email: li_zy@jlu.edu.cn; **Jun Fu**, PhD, Professor, research interest: bionic harvesting technology and equipment of grain, Email: fu_jun@jlu.edu.cn; **Qiankun Fu**, PhD, Associate Professor, research interest: modern agricultural equipment technology, Email: qkfu@jlu.edu.cn; **Xiwen Luo**, Professor, Academician of Chinese Academy of Sciences, research interest: agricultural mechanization engineering, Email: xwluo@scau.edu.cn.
***Corresponding author: Zhao Xue**, PhD, Assistant Researcher, research interest: modern agricultural equipment technology. College of Biological and Agricultural Engineering, Jilin University, Changchun 130022, China. Tel: +86-16604463765, Email: xuez@jlu.edu.cn.

In recent years, extensive research has been conducted on the structural optimization of maize peeling devices, material interaction mechanisms, and loss reduction control[8-10]. Ji et al.[11] innovatively optimized the spiral peeling roller configuration to adapt to the material characteristics of high-humidity maize in southern China, achieving loss-reducing peeling via overall structural parameter regulation. Chang et al.[12] and Chen et al.[13,14] developed a mobile peeling machine for seed maize, combining discrete element modeling and dynamic simulation to analyze the interaction law between maize ears and the mechanism, and realizing peeling loss reduction through peeling roller optimization. Du et al.[15] and Liu et al.[16,17] integrated TRIZ theory, Hertz contact theory, and discrete element simulation to focus on peeling roller configuration improvement and damage mechanism exploration, improving operational performance through overall structural optimization and mechanical analysis. Most existing studies focus on integral peeling roller improvement, operating parameter regulation, and material optimization, which only improve peeling performance in specific scenarios and fail to fundamentally solve the technical problems of high-humidity maize peeling.

The segmented combined structure has been maturely applied in modern agricultural harvesting equipment due to its advantages of functional partitioning and cooperative operation. Di et al.[18] optimized the segmented combined configuration of the maize axial flow threshing drum, and effectively reduced kernel damage and threshing residues through the cooperative operation of heterogeneous components. Wang et al.[19] optimized the maize cleaning device using a segmented sieve structure, improving material sorting quality via differentiated zonal operations. Wei et al.[20] applied a multi-segment separation structure to potato harvesting equipment, completing material transportation and soil-impurity separation in a graded manner and significantly reducing operational damage. In summary, the segmented design can adapt to the load and working condition requirements of different operation stages, serving as an effective technical approach for loss reduction and efficiency improvement of agricultural machinery. However, this design concept has rarely been applied in the field of maize peeling. Most existing peeling rollers adopt a single integral structure, lacking zonal functional configuration, and fail to combine the material characteristics of high-humidity bracts and kernels to conduct differentiated structural design for the working conditions of each stage in the entire peeling process, thus making it difficult to balance the dual technical requirements of efficient peeling and low-damage operation for high-humidity maize.

To address the above issues, high-humidity maize ears were taken as the research object in this study. A segmented combined peeling roller with low damage and high cleanliness was designed. The key structural and motion parameters were optimized. Experiments were conducted to explore the influence law of the segmented structure on peeling performance. The aim was to achieve the synergistic optimization of the bract stripping rate and kernel damage rate. A reference was provided for the optimization of maize peeling equipment.

2 Design of peeling roller

The schematic diagram of the principle of mechanical maize peeling is shown in Figure 1. During the peeling process, paired peeling rollers rotating in opposite directions tear the bracts downward by virtue of friction. When the force exerted by the peeling rollers exceeds the breaking strength of the bracts, the bracts are torn off and separated from the maize ears. The surface structural characteristics of the peeling rollers directly determine their frictional properties, which are the core factor regulating the peeling effect and grain damage. For this purpose, the optimization design of the convex rib structure and surface pattern was carried out separately in this section.

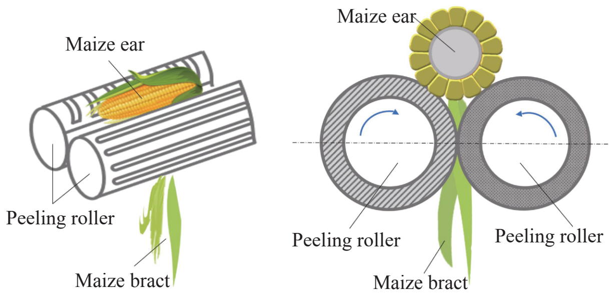

Figure 1 Schematic diagram of mechanical maize peeling

2.1 Convex rib structure design

2.1.1 Contact mechanics model between grain and convex rib

The force exerted by the convex rib structure of the peeling roller on maize grains directly affected grain damage during maize peeling. A contact mechanics model between grain and convex rib was established based on Hertz contact theory, and the contact schematic diagram is shown in Figure 2.

The critical speed for non-damage of maize grains was determined as:

$$v = \left\{ \frac{\pi^5 K_{[e,g]}^5 R^{*3} F_2(e)}{30 m E^{*4}} \right\}^{\frac{1}{2}} \tag{1}$$

where, v is the relative critical velocity at which maize kernels detach or fracture under mechanical stress, m/s; R^* is the equivalent relative radius of curvature, m; E^* is the equivalent elastic modulus, Pa; K_e and K_g are the detachment yield limit and fracture yield stress limit of maize kernels under uniaxial compression, respectively; $F_2(e)$ denotes the eccentricity geometric correction function; m is the equivalent mass of the rib-kernel contact system, kg.

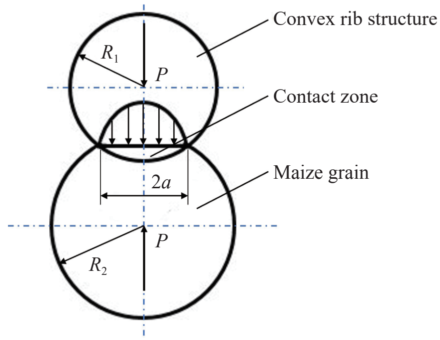

Figure 2 Schematic diagram of the contact mechanics model between grain and convex rib

It could be seen from Equation (1) that the relative critical velocity v at which maize grains underwent shedding or breakage due to mechanical stress was mainly related to the masses and elastic moduli of the two, the geometric dimensions of grains, the maximum and minimum radii of curvature of the convex rib structure on any normal plane within the contact area, as well as the shedding yield limit K_e or breaking yield stress limit K_g of maize grains under uniaxial compression.

When the material properties of maize were constant, the smaller the maximum and minimum radii of curvature of the convex rib structure on any normal plane in the contact area, and the larger the elastic modulus of the peeling roller, the smaller the relative critical velocity v required for grains to shed or break, and the more easily the grains were damaged.

2.1.2 Contact area model between grain and convex rib

The contact cross-sectional area determines the impact intensity exerted on the grain. Field investigations showed that friction and collision between fish-scale convex ribs and grains during the peeling process caused significant grain damage. The contact cross-sectional area between grains and fish-scale convex ribs was analyzed, and the contact diagram is shown in Figure 3. Assuming a compression amount h_1 was generated by elastic deformation of a grain under the force of the fish-scale convex rib structure, the maximum contact cross-sectional area S_1 was approximately a rectangle with AB (l_1) as the length and grain thickness T as the width. Assuming the grain contacted the edge of fish-scale convex ribs at an angle of 45°, the length of AB (l_1) was:

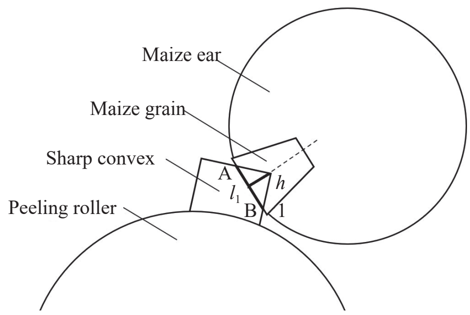

Figure 3 Analysis of contact area between grains and fish-scale roller ribs

$$l_1 = 2h_1 \tag{2}$$

The cross-sectional area S_1 formed by the contact was expressed as:

$$S_1 = 2h_1T \tag{3}$$

From Hertz contact model, increasing the radii of curvature of the convex rib structure on any normal plane in the contact area during its design can reduce grain damage. Therefore, it was considered that the convex rib structure should be designed as arc.

The schematic diagram of friction and collision contact between grains and arc convex rib is shown in Figure 4. Assuming a compression amount h_2 be generated by elastic deformation of a grain under the force of the arc convex rib structure, the maximum contact cross-sectional area S_2 is approximately a rectangle with AB (l_2) as the length and grain thickness T as the width. Let the radius of the top of the arc convex rib be R, the length of AB (l_2) is:

$$l_2 = 2\sqrt{R^2-(R-h_2)^2} \tag{4}$$

The cross-sectional area S_2 formed by the contact is expressed as:

$$S_2 = 2\sqrt{R^2-(R-h_2)^2}T \tag{5}$$

$$S_2 - S_1 = 2\sqrt{R^2-(R-h_2)^2}T - 2h_1T \tag{6}$$

When $S_2 - S_1 \geq 0$, there is:

$$R \geq h \tag{7}$$

It is known that the maximum compressive deformation h of grains when undergoing compression fracture ranges from 0.44 mm to 0.53 mm[12]. Therefore, as long as the value of R is greater than 1 mm, under the same conditions, the impact intensity of the arc convex rib structure on grains is smaller than that of the fish-scale convex rib structure, resulting in less damage to grains.

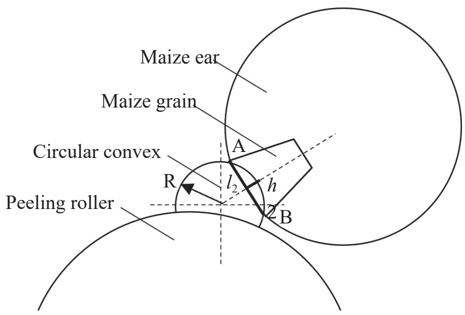

Figure 4 Analysis of contact area between grains and arc convex ribs

2.2 Surface pattern design

The surface pattern structure of peeling roller is a key factor affecting the peeling effect of maize ears and the degree of grain damage. Combined with the peeling process of maize ears in a peeling device, the surface pattern structure of peeling rollers was designed to achieve low-damage and high-cleanliness peeling of maize ears.

The operation process of maize ears on peeling rollers can be divided into three stages:

(1) Most maize bracts are removed in the front section of peeling rollers; it is necessary to increase the peeling force and peeling area of the front roller on bracts to improve peeling efficiency.

(2) Entering the middle section of peeling rollers, some ears still have a small amount of residual bracts. It is necessary to ensure that the residual bracts are peeled off, while reducing the damage of the middle roller to the peeled bare ears.

(3) Entering the rear section of peeling rollers, nearly 90% of ears have been completely peeled; at this time, the bare ears have a high sliding speed, and they are in direct contact with the peeling rollers, so reducing the damage to the bare ears is particularly important.

Therefore, the peeling roller was designed into a three-section combined type to meet the peeling requirements of the three stages. The height of the convex ribs in the three sections was reduced in turn to enhance the bract removal capacity of the front peeling roller and reduce the damage of the rear peeling roller to the bare ears. In addition, groove structures were arranged on the surface of the segmented combined peeling roller. Arc convex ribs and grooves were placed alternately to increase the peeling area of the peeling roller and improve the bract stripping rate. As the peeling roller rotated, the groove structure served as a grain overflow channel, which guided the grains shedding during peeling into the recovery box and reduced the grain breaking rate.

To avoid excessive load on individual grains from the convex rib structure, the contact width between arc convex ribs and bare ears was set to be larger than the width of a single grain[21,22], and the arc radius was calculated to be 11 mm at this time. To ensure that the shedding grains could enter the grooves of the peeling roller, the groove width was set to be larger than the grain width, and the groove depth was larger than the grain thickness. It was determined that the surface pattern of the peeling roller consisted of 12 pairs of convex rib and groove structures. The outer diameter D of the three-section peeling roller was 72 mm, and the inner diameter d was 35 mm. The heights H of the convex ribs in the three sections were 5 mm, 3.5 mm, and 2 mm, respectively, and the corresponding arc radii R were 5 mm, 6 mm, and 11 mm, respectively. The schematic diagram of the surface structure of the three-section peeling roller is shown in Figure 5.

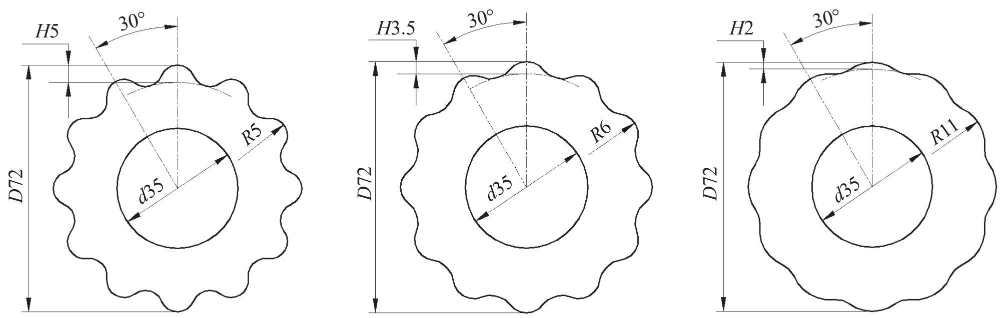

a. Front section-5 mm b. Middle section-3.5 mm c. Rear section-2 mm

Figure 5 Schematic diagram of the surface structure of the three-section peeling roller

Rubber material with a low elastic modulus was chosen for the peeling roller to reduce grain damage and meanwhile offer better grip on maize bracts. The physical prototype and overall layout of the segmented combined peeling roller are shown in Figure 6.

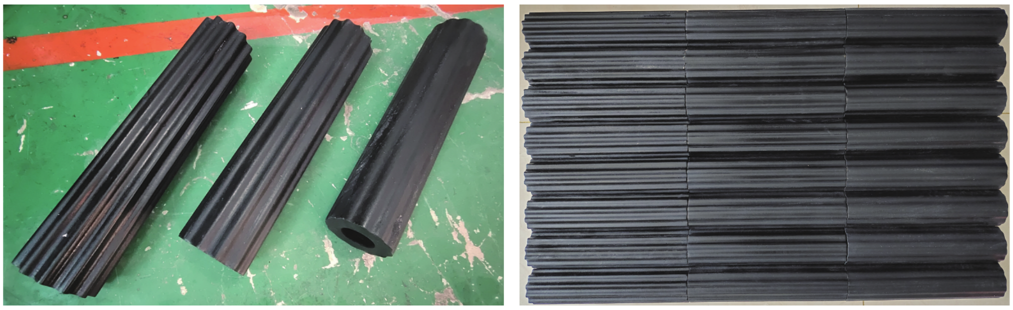

Figure 6 Physical prototype and overall layout of the segmented combined peeling roller

3 Experimental study on segmented combined peeling roller

3.1 Friction characteristic test

A self-developed multiparameter adjustable friction characteristic apparatus was established based on the structure and working principle of peeling devices[23]. It was mainly composed of a power system, pressure loading system, and data acquisition system, as shown in Figure 7. Power was transmitted from an AC motor to the peeling roller via a CYB-803S/A100 torque sensor and two couplings. The pressure loading system included a lifting mechanism, HZC-H1 load cell, pressure plate, guide plate, and material groove. The CYB-809I data acquisition system enabled real-time monitoring of the torque and speed of the peeling roller at a 100 Hz sampling frequency. Using this device, friction characteristic tests were conducted between the segmented combined peeling roller and fish-scale peeling roller at a speed of 350 r/min. Test objects included bare maize ears and maize ears with bracts. The maize variety used was Jidan 558, with a kernel moisture content of 35.24% and a bract moisture content of 38.33%.

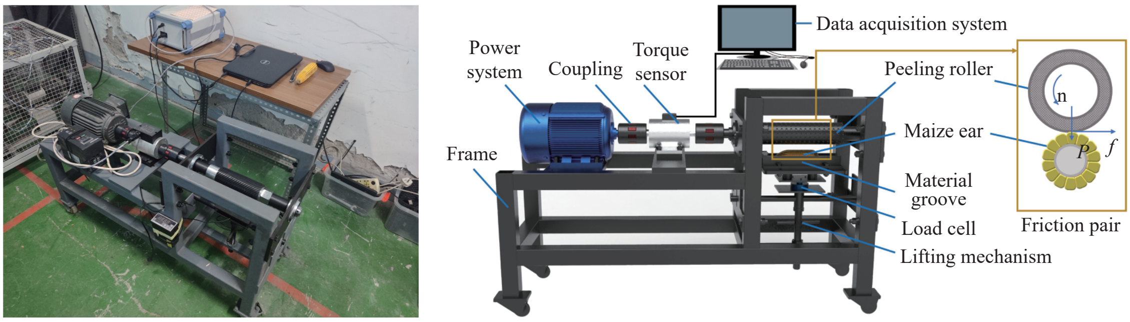

Figure 7 Friction characteristic apparatus

At the start of each test, the continuous no-load torque of the peeling roller at the test speed were recorded (attributed to the inertia of bearings and peeling roller). The formal test then commenced with preset roller speed and normal pressure P, and continuous load torque was recorded. The recorded continuous no-load and load torques were averaged to obtain T_i and T_t, respectively, and the rolling friction coefficient (μ_r) was derived from Equation (8):

$$\mu_r = \frac{T_t - T_i}{PR} \tag{8}$$

where, R is the radius of the peeling roller, mm.

3.2 Simulation analysis test

To further verify the influence law of the surface pattern structure of the segmented combined peeling roller on the force acting on maize ears, this study conducted simulation tests and analysis on three surface pattern structures of the segmented combined peeling roller based on the finite element analysis method[24,25]. The contact between the peeling roller and maize ears is a typical nonlinear problem of boundary conditions, where both the contact area and stress at the interface change with external load. Therefore, the Standard solver in Abaqus software was selected for the simulation analysis of the peeling movement[26]. According to the mechanical properties of materials, both the maize ears and the segmented combined peeling roller were defined as deformable bodies, and their contact model was simplified to a two-dimensional model[27]. The geometric models of the maize ears and the segmented combined peeling roller were established in a two-dimensional plane; the simulation analysis model is shown in Figure 8, and the corresponding material properties were assigned respectively with reference to Table 1[28].

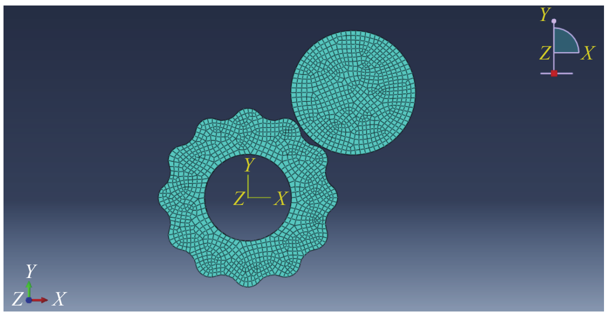

Figure 8 Diagram of simulation analysis contact

A reference point (RP) for the segmented combined peeling roller was established, and the maize ear and the segmented combined peeling roller were assembled. The interaction mode between the two was selected as surface-to-surface. Referring to the results of the friction characteristics test, the friction coefficients of the contact surfaces between the maize ear and the three-section peeling roller were set to 0.322, 0.308, and 0.284, respectively.

Table 1 Material properties

Property	Maize ear	Compounded rubber
Poisson's ratio	0.4	0.47
Elasticity modulus/MPa	364	7.8

3.3 Orthogonal optimization test

To achieve low-damage and high-cleanliness peeling effect of maize ears, this study carried out operation parameter optimization tests of the segmented combined peeling roller with the peeling roller speed, the pressing wheel speed, and the distance between peeling roller and pressing wheel.

3.3.1 Test materials and equipment

The maize ears used in the experiment were from the Agricultural Experimental Base of Jilin University (43°56′N, 125°14′E) in Changchun, Jilin province, China. The maize variety was Jidan 558. The maize ears were picked manually to avoid the influence of mechanical damage on the test results. The moisture contents of grains and bracts, determined by drying method, were 32.14% and 36.39%, respectively.

Tests were conducted on a maize peeling test bench, as shown in Figure 9. The bench mainly consisted of an industrial computer, power unit, maize peeling device, conveyor, and an additional set of AC motor and frequency converter. The designed segmented combined peeling roller was installed in the maize peeling device. The YVF2-280M-4 AC motor and SVF-G7 frequency converter in the power unit served as the drive for the peeling roller group and regulated its rotational speed, respectively. The YE290L-2 motor drove the pressing wheel, with its speed adjusted by the FR150-2S-2.2B frequency converter.

Figure 9 Maize peeling test bench

3.3.2 Test method and design

Prior to testing, maize ears were placed on the conveyor. The structure and motion parameters of the peeling device were adjusted in accordance with the test scheme. After the device operated stably, the conveyor was started and set to the specified test speed. maize ears were conveyed into the peeling device inlet, and the peeled ears fell into the collection box via the outlet. Based on the field operation speed of maize harvesters and plant spacing, the feeding rate was set at 10 ears per second, with 50 ears tested per group. Each trial ended once all ears exited the outlet. To ensure result reliability, each test was repeated three times, and the average value was adopted.

According to the industry standard B/T 11907-2014 for maize husker, grain shedding rate S, grain breaking rate P, and bract stripping rate J were selected as performance evaluation indices of the segmented combined peeling roller, with the calculation Equations given below:

Grain shedding rate (%):

$$S = \frac{G_s}{G + G_s} \times 100\% \tag{9}$$

Grain breaking rate (%):

$$P = \frac{G_p}{G + G_s} \times 100\% \tag{10}$$

Bract stripping rate (%):

$$J = \left(1 - \frac{n_b}{n}\right) \times 100\% \tag{11}$$

where, G_s is the mass of grains shedding from maize ears during peeling, g; G_p is the mass of grains in the collection box after peeling, g; G is the mass of breaking grains, g; n_b is the number of maize ears remaining with more than 3 bracts after peeling; n is the total number of test maize ears per trial.

The three-factor and three-level Box-Behnken response surface design was employed in this study[29-31]. Test factors and coded levels were determined based on field operational parameters of domestic and overseas maize harvesters[32] and preliminary test results, as listed in Table 2.

Table 2 Test factors and coded levels

Level	Factor		
	Peeling roller speed x_1/r·min^{-1}	Pressing wheel speed x_2/r·min^{-1}	Distance between peeling roller and pressing wheel x_3/mm
–1	300	60	25
0	350	80	30
1	400	100	35

3.4 Field validation test

Based on the orthogonal test results of the segmented combined peeling roller, a field test was performed to verify the optimal operation parameters, with a comparison to the conventional fish-scale spiral peeling roller to confirm the superiority of the designed roller. Two maize ear harvesters from Shandong Juming Machinery Co., Ltd. were used: the 4YZP-4Y (equipped with conventional fish-scale spiral peeling rollers) and 4YZLP-2C (equipped with the proposed segmented combined peeling rollers), as shown in Figure 10. Except for differences in operating row number and traveling devices, other structural components were identical to ensure reliable and comparable test results.

a. 4YZP-4Y maize ear harvester b. 4YZLP-2C maize ear harvester

Figure 10 Validation test in field

The test maize variety was Jidan 56, with grain and bract moisture contents of 33.27% and 38.44%, respectively. The field test strictly followed GB/T 21692-2020 maize combine harvester. The test field had a maize plant spacing of 24 cm and row spacing of 55 cm. Lodging plants in the measurement area were manually cleaned before the test to avoid affecting the test effect. Each operation distance was 20 m. Each group of tests was repeated three times, and the average value was taken.

4 Results and discussion

4.1 Results and discussion of friction characteristic test

The test simulated the operation process of maize ears rolling around their own axes under the friction force of the peeling rollers, and the test results are listed in Table 3. It could be seen from Table 3 that the rolling friction coefficients between the segmented combined peeling roller and the maize ear decreased sequentially from the front section to the rear section, which could meet the design requirements of enhancing the bract stripping capacity in the front section and reducing the damage of bare ears in the rear section. In addition, under the same moisture content condition, compared with the fish-scale peeling roller, the segmented combined peeling roller designed in this study increased the equivalent friction coefficient with the maize ears with bracts, which was conducive to improving the bract stripping efficiency; it also reduced the equivalent friction coefficient with the bare maize ears, effectively reducing grain damage during operation.

4.2 Results and discussion of simulation analysis test

The test simulated the forces acting on maize ears during the peeling process. The degrees of freedom of the upper part and the right side of the maize ear were constrained. The peeling roller was set to contact the maize ear in the vertical direction. The moving distance *d* was set to 5 mm. The model was divided into global meshes with an approximate global element size of 1. After submitting the simulation job, the stress nephograms of the three-section peeling rollers with convex rib heights of 5 mm, 3.5 mm, 2 mm and the maize ear under different moving distances *d* were obtained, as shown in Figure 11. Among them, states Ⅰ, Ⅱ, and Ⅲ correspond to moving distances d=1 mm, d=3 mm, and d=5 mm, respectively.

According to the analysis results of the stress nephograms, the maximum stresses at the contact between the maize ear and the peeling rollers with convex rib heights of 5 mm (front section), 3.5 mm (middle section), and 2 mm (rear section) were 2.59 MPa, 2.46 MPa, and 2.18 MPa, respectively. The maximum stress of the ear was concentrated in the rib contact area. Under the established simulation conditions, the larger the rib height and the smaller the top arc radius, the higher the stress on the maize ear. The simulation results were consistent with the theoretical analysis rules. The 5 mm convex rib in the front section could provide greater contact stress, which was conducive to bract stripping and improving the stripping rate; reducing the convex rib height and increasing the top arc radius of the ribs could significantly reduce the stress amplitude of the ear. When the ears entered the rear section of the peeling roller, nearly 90% of the bracts had been stripped, and the bare ears were in direct contact with the peeling roller. A smaller convex rib height could effectively reduce the kernel damage rate. The results showed that the designed segmented combined peeling roller could meet the requirements of high bract stripping rate and low damage for maize ear peeling operation.

Table 3 Results of friction characteristics test

Maize sample	Rolling friction coefficient			
	Segmented combined peeling roller			Fish-scale spiral peeling roller
	Front section	Middle section	Rear section	
Bare maize ear	0.331	0.313	0.290	0.334
Maize ear with bracts	0.322	0.308	0.284	0.293

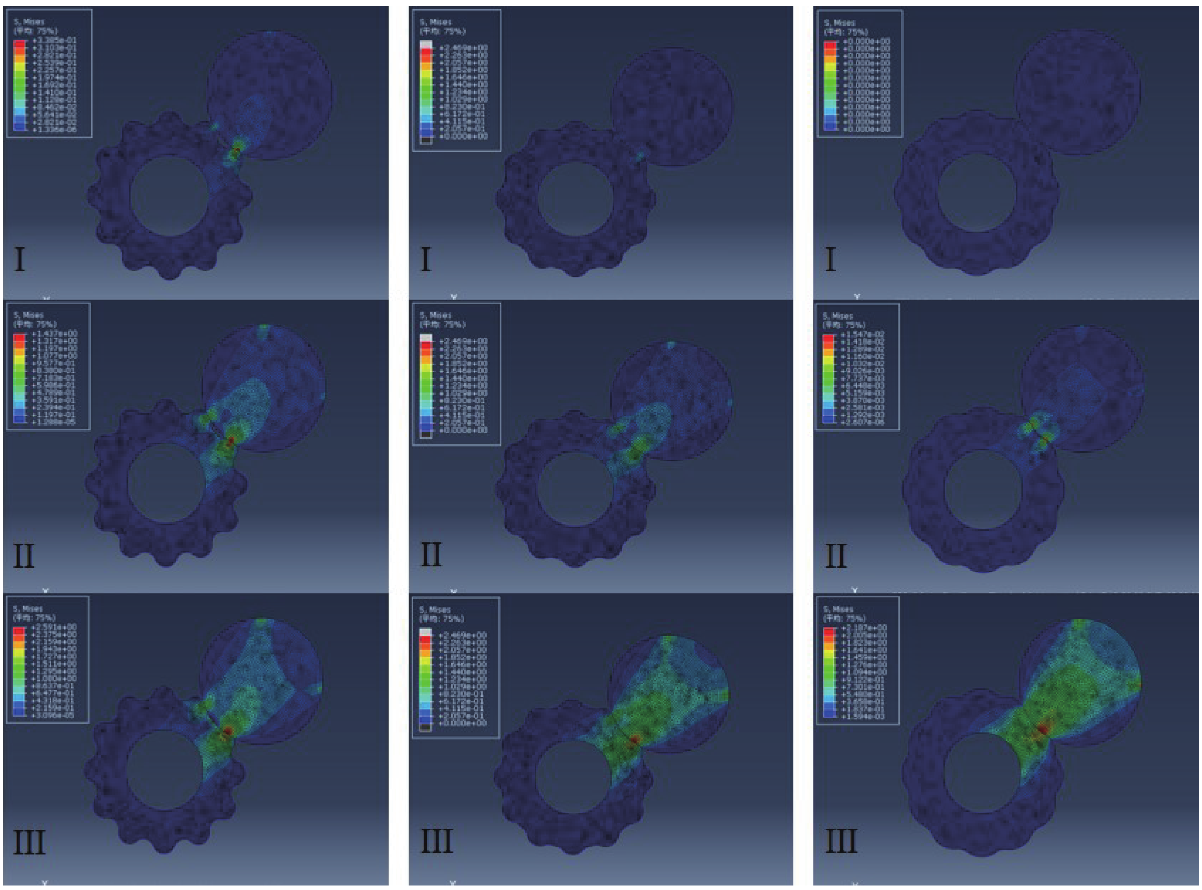

a. Front section-5 mm b. Middle section-3.5 mm c. Rear section-2 mm

Figure 11 Contact stress nephogram of segmented combined peeling roller and maize ear

4.3 Results and discussion of orthogonal optimization test

4.3.1 Test results and regression analysis

Design-expert 8.0.6.1 software was used for test design and data analysis. The test scheme and results are listed in Table 4.

Table 4 Results and design of test

Level	Factor			Bract stripping rate	Grain shedding rate	Grain breaking rate
	x_1	x_2	x_3	y_1/%	y_2/%	y_3/%
1	–1	–1	0	86	1.39	0.45
2	1	–1	0	84	1.11	0.85
3	–1	1	0	84	1.38	0.46
4	1	1	0	98	1.53	0.72
5	–1	0	–1	84	1.08	0.42
6	1	0	–1	96	1.34	0.93
7	–1	0	1	88	1.48	0.51
8	1	0	1	96	1.06	0.69
9	0	–1	–1	86	1.13	0.67
10	0	1	–1	94	1.25	0.65
11	0	–1	1	96	1.23	0.69
12	0	1	1	96	1.36	0.56
13	0	0	0	98	0.91	0.52
14	0	0	0	98	0.89	0.48
15	0	0	0	96	0.90	0.50
16	0	0	0	100	0.87	0.51
17	0	0	0	96	0.89	0.52

Design-expert software was used for quadratic regression response analysis of the test data to establish quadratic regression models between the bract stripping rate (y_1), grain shedding rate (y_2), grain breaking rate (y_3) and each test factor. Analysis of variance (ANOVA) was performed on the three models and their factor terms (Table 5). The results indicated that the three models were extremely significant, with F-values of 13.70, 119.58, and 122.00, and corresponding p-values of 0.0012, <0.0001, and <0.0001, respectively. The p-values of the lack-of-fit terms for all models were greater than 0.05, demonstrating good model fitting effects. After eliminating insignificant terms (p>0.10, NS) and refitting, the final fitting relationships between each performance index and test parameters were obtained as follows:

$$y_1 = -188.473\,68 + 1.395\,79x_1 + 0.261\,84x_2 + 0.4x_3 + 4\times10^{-3}x_1x_2 - 2.336\,84\times10^{-3}x_1^2 - 9.605\,26\times10^{-3}x_2^2 \quad (12)$$

$$y_2 = 15.647\,25 - 0.053\,045x_1 - 0.126\,10x_2 - 0.039\,350x_3 + 1.075\times10^{-4}x_1x_2 - 6.8\times10^{-4}x_1x_3 + 9.16\times10^{-5}x_1^2 + 5.7875\times10^{-4}x_2^2 + 4.76\times10^{-3}x_3^2 \quad (13)$$

Table 5 Analysis of variance for regression models

Source of variation	Bract stripping rate		Grain shedding rate		Grain breaking rate	
	F-value	p-value	F-value	p-value	F-value	p-value
Model	13.70	0.0012**	119.58	<0.0001**	122.00	<0.0001**
x_1	30.68	0.0009**	14.14	0.0071**	743.44	<0.0001**
x_2	11.99	0.0105*	73.23	<0.0001**	29.74	0.0010**
x_3	7.67	0.0277*	18.31	0.0037**	19.74	0.0030**
x_1x_2	15.34	0.0058**	62.17	0.0001**	15.99	0.0052**
x_1x_3	0.96	0.3601NS	155.47	<0.0001**	88.85	<0.0001**
x_2x_3	3.84	0.0910	0.034	0.8597NS	9.87	0.0163*
x_1^2	33.96	0.0006**	296.95	<0.0001**	40.81	0.0004**
x_2^2	14.58	0.0066**	303.47	<0.0001**	48.65	0.0002**
x_3^2	0.65	0.4480NS	80.19	<0.0001**	81.47	<0.0001**

Note: p < 0.01 (**) was very significant; p < 0.05 (*) was significant; and p > 0.10 (NS) was not significant.

$$y_3 = 0.914\,25 + 8.15\times10^{-4}x_1 - 4.9875\times10^{-3}x_2 - 0.0528x_3 - 3.5\times10^{-5}x_1x_2 - 3.3\times10^{-4}x_1x_3 - 2.75\times10^{-4}x_2x_3 + 2.18\times10^{-5}x_1^2 + 1.4875\times10^{-4}x_2^2 + 3.08\times10^{-3}x_3^2 \quad (14)$$

4.3.2 Response surface analysis

Significant differences in operational performance of the segmented combined peeling roller were observed under various parameter conditions. Design-expert software was adopted for response surface analysis of test data to clarify the influence rules of each test factor on operational performance and determine the optimal parameter combination.

(1) Influence of test factors on bract stripping rate

The response surfaces of various factors affecting the bract stripping rate were analyzed (Figure 12). The interaction intensity of factor pairs was ranked as: x_1x_2>x_2x_3> x_1x_3, which was consistent with the ANOVA results. The analysis indicated that both peeling roller speed and pressing wheel speed exerted an effect on the bract stripping rate with an initial increasing and subsequent decreasing trend. The bract stripping rate declined as the distance between peeling roller and pressing wheel increased. Accordingly, the optimal parameter combination for maximizing the bract stripping rate (y_1) was determined as: x_1=374.72 r/min, x_2=90.17 r/min, and x_3=31.53 mm.

(2) Influence of test factors on grain shedding rate

Response surfaces of various factors affecting the grain shedding rate were analyzed (Figure 13). The interaction intensity

of factor pairs was ranked as: x_1x_3>x_1x_2>x_2x_3, which agreed well with the ANOVA results. A consistent variation trend of grain shedding rate was presented in Figures 13a-13c. The grain shedding rate first decreased and then increased with the rise of peeling roller speed, pressing wheel speed, and distance between peeling roller and pressing wheel. The optimal parameter combination for the minimum grain shedding rate (y_2) was determined as: x_1=354.22 r/min, x_2=76.06 r/min, and x_3=29.45 mm.

(3) Influence of test factors on grain breaking rate

Response surfaces of various factors affecting the grain breaking rate were analyzed (Figure 14). The interaction intensity of factor pairs was ranked as: x_1x_3>x_1x_2>x_2x_3, which was consistent with the ANOVA results. The analysis indicated that peeling roller speed was the dominant factor affecting grain breaking rate, which increased significantly as the speed increased. Both pressing wheel speed and distance between peeling roller and pressing wheel exhibited an initial decreasing followed by an increasing trend in grain breaking rate. The optimized parameter combination for the minimum grain breaking rate (y_3) was obtained as: x_1=301.02 r/min, x_2=82.16 r/min, and x_3=29.66 mm.

4.3.3 Determination of optimal operating parameters

Maize peeling operation needs to simultaneously meet the comprehensive performance requirements of high bract stripping rate, low grain shedding rate, and low grain breaking rate. In this study, the primary objective function method of multi-objective optimization was adopted to comprehensively optimize the operating parameters[33,34]. Combined with the actual production requirements, different weights were assigned to each index in the optimization model. The bract stripping rate was set as the highest priority, followed by the grain breaking rate, and the grain shedding rate as the lowest priority. Numerical optimization was conducted via Design-expert software to obtain the optimal parameter combination satisfying the operational performance[35], and the objective function is expressed as follows:

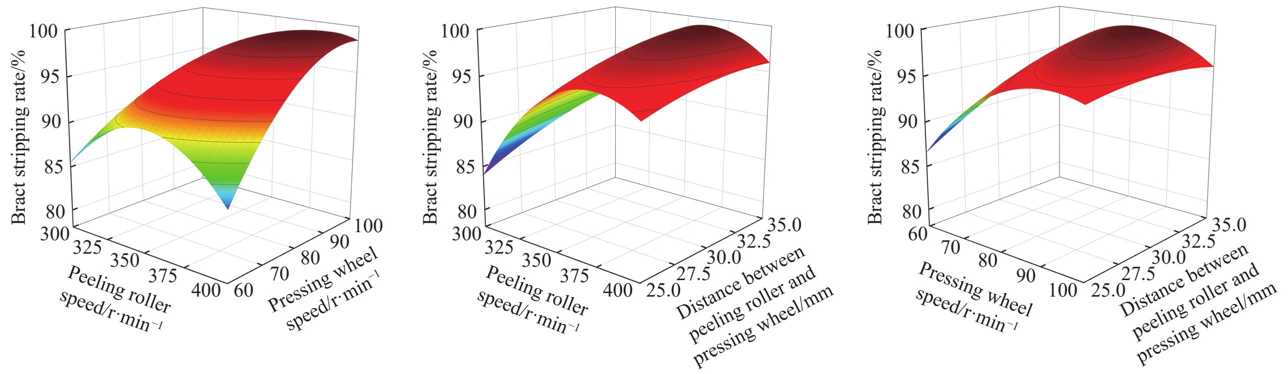

a. $y_1=f(x_1, x_2, 30)$ b. $y_1=f(x_1, 80, x_3)$ c. $y_1=f(350, x_2, x_3)$

Figure 12 Effects of interactive factors on bract stripping rate

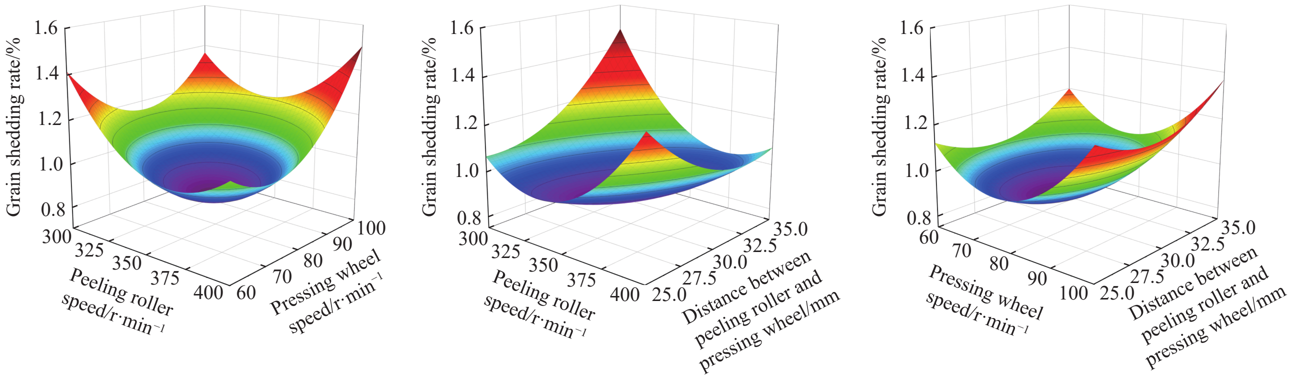

a. $y_2=f(x_1, x_2, 30)$ b. $y_2=f(x_1, 80, x_3)$ c. $y_2=f(350, x_2, x_3)$

Figure 13 Effects of interactive factors on grain shedding rate

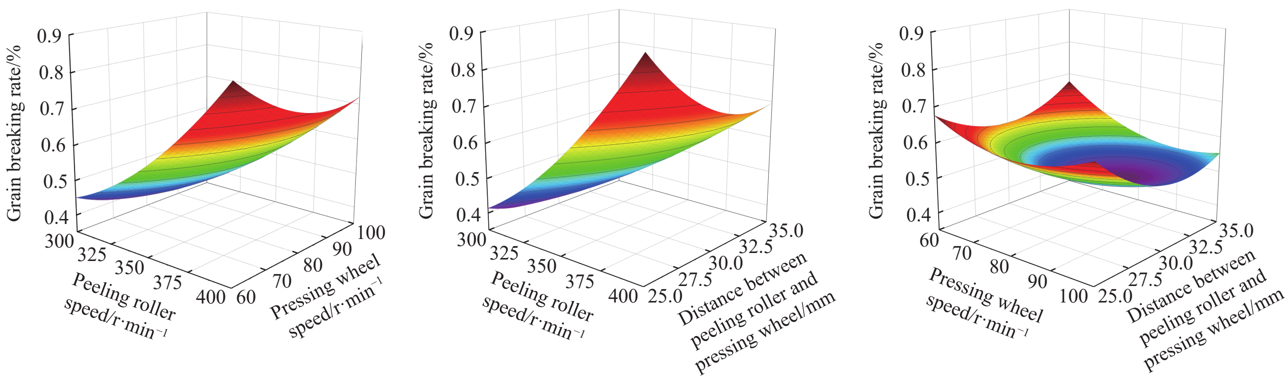

a. $y_3=f(x_1, x_2, 30)$ b. $y_3=f(x_1, 80, x_3)$ c. $y_3=f(350, x_2, x_3)$

Figure 14 Effects of interactive factors on grain breaking rate

$$\begin{cases} \max y_1, \\ \min y_2 \\ \min y_3 \\ 300\ \mathrm{r/min} \le x_1 \le 400\ \mathrm{r/min} \\ 60\ \mathrm{r/min} \le x_2 \le 100\ \mathrm{r/min} \\ 25\ \mathrm{mm} \le x_3 \le 35\ \mathrm{mm} \end{cases} \tag{15}$$

After multi-objective optimization calculation, the optimal structural and motion parameter combination of the segmented combined peeling roller was determined as follows: x_1=353 r/min, x_2=82 r/min, and x_3=31 mm.

4.4 Results and discussion of field validation test

Field validation test results are presented in Table 6. It could be seen from the test results that the average bract stripping rate of the segmented combined peeling roller was 93.80%, with the grain shedding rate and grain breaking rate reaching 0.96% and 0.54%, respectively. Small relative errors were found between the test values and the model predicted values, which confirmed the reliability of the optimization model. Compared with the conventional fish-scale spiral peeling roller, the newly designed segmented combined peeling roller increased the bract stripping rate by 10.89%, while the grain shedding rate and grain breaking rate decreased by 68.93% and 63.51%, respectively. The overall peeling performance was effectively improved, and satisfactory operational stability was maintained under the optimal parameter combination in field conditions.

Table 6 Field validation test results

Test index/%	Segmented combined peeling roller			Fish-scale spiral peeling roller
	Field test value	Model predicted value	Relative error	
Bract stripping rate	93.80	98.45	4.96	84.59
Grain shedding rate	0.96	0.92	4.17	3.09
Grain breaking rate	0.54	0.51	5.56	1.48

5 Conclusions

To address the technical bottlenecks of high grain damage rate and low bract stripping rate in maize peeling operations, a low-damage and high-cleanliness segmented combined peeling roller was designed. The operational performance of the designed peeling roller was systematically validated through friction characteristic test, simulation analysis test, orthogonal optimization test, and field validation test. The specific conclusions are as follows:

1) Based on the cross-sectional contact model between roller convex ribs and maize ears, combined with the actual peeling process of ears inside the peeling device, the structure and dimensions of convex ribs were optimized. An arc convex rib-groove structure and a three-section combined configuration were proposed. The key structural parameters of each section were determined via theoretical analysis, which provided reliable theoretical support for the peeling roller design.

2) Using a self-developed friction characteristic apparatus, the rolling friction coefficient between the three-section peeling roller and maize ears was measured. The results showed that the rolling friction coefficient decreased gradually from the front to the rear section. Simulation results further indicated that the contact stress generated between convex ribs and maize ears also declined sequentially from the front to the rear section, verifying the rationality of the structural design of the segmented combined peeling roller.

3) The Box-Behnken response surface methodology was used to systematically investigate the effects of the test factors on the operational performance of the segmented combined peeling roller. Regression models were established between the test factors and three evaluation indices. The optimal parameter combination was determined as follows: peeling roller speed of 353 r/min, pressing wheel speed of 82 r/min, and distance between peeling roller and pressing wheel of 31 mm. Under the optimal parameters, the bract stripping rate exceeded 90%, and the grain damage rate was controlled below 1%, achieving the objective of low-damage and high-cleanliness maize peeling operation.

Acknowledgements

This work was financially supported by the National Key Research and Development Program of China (Grant No. 2024YFD2000103), and the Jilin Provincial Integrated Pilot Project for Agricultural Machinery R&D, Manufacturing, Promotion, and Application of Lightweight and Simplified maize Harvesters for Hilly and Mountainous Areas.

[References]

[1] Zhao C H, Zhao T, Hu B L. Design and experimental study of the multi-function corn peeling machine with analysis of segmented metal construction materials. Advanced Materials Research Application, 2012; 600: 144–147.

[2] Fu J, Yuan H K, Zhao R Q, Chen Z, Ren L Q. Peeling damage recognition method for corn ear harvest using RGB image. Applied Sciences-Basel, 2020; 10(10): 3371.

[3] Zhu Z X, Yue X W, Du Y F, Song Z H, Mao E R, et al. Dynamic simulation and high-speed photography experiment on corn-ear husking. Transactions of the CSAE, 2015; 31(6): 42–48. (in Chinese)

[4] Zhou J L, Jian S C, Wei G J, Hao F P, Jiang W, Di Z F, et at. Research on the five factors corn husker experiment device and test scheme design. Journal of Agricultural Mechanization Research, 2016; 38(3): 167–173. (in Chinese)

[5] Li Z Y, Fu J, Luo X W. Tensile properties and fracture mechanisms of maize bract for corn peeling device design. Agriculture-Basel, 2021; 11(8): 0796.

[6] Yang F, Du Y F, Fu Q F, Li X Y, Li Z, Mao E R, et al. Design and testing of seed maize ear peeling roller based on Hertz theory. Biosystems Engineering, 2021; 202: 165–178.

[7] Takawira-Nyakuchena M, Mushiri T, Seliger G, Ganiyusufoglu O S, Zhang W, Kohl H. Design of an automated maize de-husking machine for the case of Zimbabwe. Procedia Manufacturing, 2020; 43: 127–134.

[8] Dai Z Y, Wang Y. Effects of physical and mechanical properties of corn ear on working performance of husking device. Transactions of the CSAM, 1992; 23(4): 86–89. (in Chinese)

[9] Dai Z Y, Qu J X. The test for selecting the type and parameters of ear-corn husking roll. Transactions of the CSAM, 1995; 26(2): 58–62. (in Chinese)

[10] Chen M Z, Xu G F, Wei Y Z, Zhang Y P, Diao P S, Pang H X. Design and experiment analysis of the small maize harvester with attitude adjustment in the hilly and mountainous areas of China. Int J Agric & Biol Eng, 2024; 17(1): 118–127.

[11] Ji B, Pan L, Wang Z K, Xie F P, Xie Y S, Wu B. Design and test of corn cob peeling device for high moisture content in southern China. Transactions of the CSAM, 2026; 57(7): 239–250. (in Chinese)

[12] Chang L L, Zhao W Y, Shi R J, Dai F, Liu X L, Ren X J. Development and experimental validation of flexible discrete element model for seed maize ears. Transactions of the CSAM, 2026; 57(8): 173–182, 192. (in Chinese)

[13] Chen J Z, Shi R J, Dai F, Zhao W Y, Zhao Y M, Xin S L. Simulation and experiment on interaction process between seed corn and corn husking mechanism. Transactions of the CSAM, 2024; 55(04): 91–100. (in Chinese)

[14] Chen J Z, Shi R J, Dai F, Zhao W Y, Chang L L, Yang T. Design and experiment of mobile seed corn husker. Transactions of the CSAM, 2025; 56(05): 331–342. (in Chinese)

[15] Du Y F, He S, Mao E R, Zhu Z X, Li X Y, Yang F. Design of corn ear peeling device based on knowledge-based engineering. Transactions of the CSAM, 2020; 51(S2): 249–260. (in Chinese)

[16] Liu L, Du Y F, Li X Y, Liu L H, Zhang Y A, Yang F. Analysis and experiment on kernel loss of seed corn during peeling based on EDM. Transactions of the CSAM, 2022; 53(S2): 28–38. (in Chinese)

[17] Liu L, Liu L H, Du Y F, Mao E R, Zhang Y A, Yang F. Design and experiment of seed corn peeling mechanism based on TRIZ theory. Transactions of the CSAM, 2022; 53(9): 131–141. (in Chinese)

[18] Di Z F, Cui Z K, Zhang H, Zhou J, Zhang M Y, Bu L X. Design and experiment of rasp bar and nail tooth combined axial flow corn threshing cylinder. Transactions of the CSAE, 2018; 34(1): 28–34. (in Chinese)

[19] Wang L J, Ma Y, Feng X, Song L L, Chai J. Design and experiment of segmented vibrating screen in cleaning device of maize grain harvester. Transactions of the CSAM, 2020; 51(9): 89–100. (in Chinese)

[20] Wei Z C, Li H W, Sun C Z, Li X Q, Su G L, Liu W Z. Design and experiment of potato combined harvester based on multi-stage separation technology. Transactions of the CSAM, 2019; 50(1): 129–140, 112. (in Chinese)

[21] Zhang N, Fu J, Wang R X, Chen Z, Fu Q K, Chen X G. Experimental study on the particle size and weight distribution of the threshed mixture in corn combine harvester. Agriculture-Basel, 2022; 12(8): 1214.

[22] Wang Y, Wang X M, Chen Z R, Yu J Q. Modeling method of maize kernels based on discrete element method. Journal of Jilin University (Engineering and Technology Edition), 2018; 48(5): 1537–1547. (in Chinese)

[23] Li Z Y, Fu J, Luo X W, Fu Q K, Chen Z, Ren L Q. Determination of friction characteristics of corn ears at varying factors in mechanical peeling. Journal of Food Process Engineering, 2024; 47(11). doi: 10.1111/jfpe.14764

[24] Ma S, Xu L M, Xing J J, Yuan Q C, Duan Z Z, Yu C C, et al. Study on collision damage experiment of grape and finite element analysis. Journal of China Agricultural University, 2018; 23(11): 180–186. (in Chinese)

[25] Zhang S L, Dai F, Zhao W Y, Zhang X K, Wei W C, et al. Finite element analysis of dynamic interaction between the soil-rolling device of whole film double ditch laminating machine and seedbed. Journal of China Agricultural University, 2019; 24(9): 147–159. (in Chinese)

[26] Zhuang Z, You X C, Liao J H, Cen S. Finite element analysis and application based on ABAQUS. Tsinghua University Press: Beijing, China, 2009.

[27] Fu J, Zhang Y C, Chen Z, Ren L Q, Cheng C. Bionic design and experiment of threshing tooth based on structure of cattle apex tongue

filiform papilla. Transactions of the CSAM, 2019; 50(7): 167–176. (in Chinese)

[28] Zhang L. Theoretical analysis and simulation research on novel bionic corn-ear snapping mechanism. Changchun: College of Biological and Agricultural Engineering, Jilin University, 2015.

[29] Fu Q K, Fu J, Wang F D, Chen Z, Ren L Q. Design and parameter optimization of corn head with wheel type rigid-flexible coupling snapping device to reduce loss. Transactions of the CSAE, 2019; 35(7): 21–30. (in Chinese)

[30] Ren L Q. Design of experiment and optimization. Higher Education Press: Beijing, China, 2009.

[31] Chen Y, He J, Yu X, Ma H, Wang S, Zhang X, et al. Calibration and experiment of the discrete element parameters of watermelon seeds. Int J Agric & Biol Eng, 2025; 18(4): 26–37.

[32] Xu L M, Wang Y B, Zhang D X, Zhao C S, Hou Y L. Design and experiment of corn universal husker mechanism. Transactions of the CSAM, 2011; 42(S1): 14–20. (in Chinese)

[33] Fu J, Yuan H K, Zhang D P, Chen Z, Ren L Q. Multi-objective optimization of process parameters of longitudinal axial threshing cylinder for frozen corn using RSM and NSGA-II. Applied Sciences-Basel, 2020; 10(5): 1646.

[34] Zhang N, Fu J, Chen Z, Chen X G, Ren L Q. Optimization of the process parameters of an air-screen cleaning system for frozen corn based on the response surface method. Agriculture-Basel, 2021; 11(8): 0794.

[35] Fu J, Li J, Tang X L, Wang R X, Chen Z. Optimization of structure parameters of the grouser shoes for adhesion reduction under black soil. Agriculture-Basel, 2021; 11(8): 0795.